REPORT DOCUMENTATION PAGE

Form Approved OMB NO. 0704-0188

1. REPORT DATE (DD-MM-YYYY)	2. REPORT TYPE	3. DATES COVERED (From - To)
13-11-2015	Final Report	15-Aug-2012 - 14-Aug-2015

4. TITLE AND SUBTITLE

Final Report: Biophysical Model of Cortical Network Activity and the Influence of Electrical Stimulation.

5a. CONTRACT NUMBER
W911NF-12-1-0418

5b. GRANT NUMBER

5c. PROGRAM ELEMENT NUMBER
611102

6. AUTHORS
William S. Anderson, Pawel Kudela

5d. PROJECT NUMBER

5e. TASK NUMBER

5f. WORK UNIT NUMBER

7. PERFORMING ORGANIZATION NAMES AND ADDRESSES
Johns Hopkins University
Physics & Astronomy
3400 North Charles Street
Baltimore, MD 21218 -2685

8. PERFORMING ORGANIZATION REPORT NUMBER

9. SPONSORING/MONITORING AGENCY NAME(S) AND ADDRESS (ES)
U.S. Army Research Office
P.O. Box 12211
Research Triangle Park, NC 27709-2211

10. SPONSOR/MONITOR'S ACRONYM(S)
ARO

11. SPONSOR/MONITOR'S REPORT NUMBER(S)
62595-MA.15

12. DISTRIBUTION AVAILIBILITY STATEMENT
Approved for Public Release; Distribution Unlimited

13. SUPPLEMENTARY NOTES
The views, opinions and/or findings contained in this report are those of the author(s) and should not contrued as an official Department of the Army position, policy or decision, unless so designated by other documentation.

14. ABSTRACT
We examined the effects of subdural electrical stimulation on a high-density network consisting of several populations of multicompartment cell types. The results can be summarized as follows: 1) Electrical stimulation mainly affects and activates axon initial and the most distal axonal segments in neurons. The most distal axonal segments are locations where presynaptic action potentials can originate regardless of the state of the axon initial segment (i.e. depolarization, hyperpolarization) 2) The effect of dendritic arbor structure on the axonal activation threshold is most prominent in the case of multipolar neurons with large diameter basal/apical dendrites that are

15. SUBJECT TERMS
neocortex, electrical stimulation, computer network model, multicompartment model, subdural cortical stimulation, anode, cathode, epilepsy

16. SECURITY CLASSIFICATION OF:			17. LIMITATION OF ABSTRACT	15. NUMBER OF PAGES	19a. NAME OF RESPONSIBLE PERSON
a. REPORT	b. ABSTRACT	c. THIS PAGE			William Anderson
UU	UU	UU	UU		19b. TELEPHONE NUMBER 443-287-4576

Report Title

Final Report: Biophysical Model of Cortical Network Activity and the Influence of Electrical Stimulation.

ABSTRACT

We examined the effects of subdural electrical stimulation on a high-density network consisting of several populations of multicompartment cell types. The results can be summarized as follows: 1) Electrical stimulation mainly affects and activates axon initial and the most distal axonal segments in neurons. The most distal axonal segments are locations where presynaptic action potentials can originate regardless of the state of the axon initial segment (i.e. depolarization, hyperpolarization) 2) The effect of dendritic arbor structure on the axonal activation threshold is most prominent in the case of multipolar neurons with large-diameter basal/apical dendrites that are oriented parallel to the electric field lines. 3) The timing of presynaptic terminal activation in neurons subjected to electrical stimulation is not solely determined by the axonal delay (i.e. orthodromic propagation) but rather depends on the details of the applied stimulation field, axonal branching structure and axon orientation in respect to the electrode position. 4) A single stimulation pulse causes a sequence of action potentials ectopically generated in axons, which in turn produce a temporal variation in the timing of postsynaptic neurons activation.

Enter List of papers submitted or published that acknowledge ARO support from the start of the project to the date of this printing. List the papers, including journal references, in the following categories:

(a) Papers published in peer-reviewed journals (N/A for none)

Received	Paper
11/05/2015 12.00	Ishita Basu, Pawel Kudela, Anna Korzeniewska, Piotr J Franaszczuk, William S Anderson. A study of the dynamics of seizure propagation across micro domains in the vicinity of the seizure onset zone, Journal of Neural Engineering, (08 2015): 46016. doi: 10.1088/1741-2560/12/4/046016
11/05/2015 13.00	Pawel Kudela, William S. Anderson. Computational Modeling of Subdural Cortical Stimulation: A Quantitative Spatiotemporal Analysis of Action Potential Initiation in a High-Density Multicompartment Model, Neuromodulation: Technology at the Neural Interface, (10 2015): 552. doi: 10.1111/ner.12327
TOTAL:	**2**

Number of Papers published in peer-reviewed journals:

(b) Papers published in non-peer-reviewed journals (N/A for none)

Received	Paper
TOTAL:	

Number of Papers published in non peer-reviewed journals:

(c) Presentations

Number of Presentations: 0.00

Non Peer-Reviewed Conference Proceeding publications (other than abstracts):

Received	Paper

TOTAL:

Number of Non Peer-Reviewed Conference Proceeding publications (other than abstracts):

Peer-Reviewed Conference Proceeding publications (other than abstracts):

Received	Paper	
09/02/2014	7.00	Ishita Basu, Pawel Kudela, William S. Anderson. Determination of seizure propagation across microdomainsusing spectral measures of causality, 36th Annual International IEEE EMBS Conference. 30-AUG-14, . : ,
11/05/2015	14.00	D. L. BOOTHE, A. B. YU, P. KUDELA, N. E. ZANDER, Y. R. SLIOZBERG, T. CHANTAWANSRI, R. J. BANTON, T. N. PIEHLER, J. M. VETTEL, W.S. ANDERSON, P. J. FRANASZCZUK. Impact of blast-dependent cellular damage on the local field potential (lfp) in a large scalesimulation of cerebral cortex, Society for Neuroscience. 19-OCT-15, . : ,

TOTAL: **2**

Number of Peer-Reviewed Conference Proceeding publications (other than abstracts):

(d) Manuscripts

Received		Paper
06/06/2013	1.00	William Anderson, Pawel Kudela, Jounhong Cho, Gregory Bergey, Piotr Franszczuk. Studies of stimulus parameters for seizure disruption using neural network simulations, Biological Cybernetics (08 2007)
06/11/2013	2.00	W.S. Anderson, P. Kudela, S. Weinberg, G.K. Bergey, P.J. Franaszczuk. Phase-dependent stimulation effects on bursting activity in a neural network cortical simulation, Epilepsy Research (07 2008)
06/12/2013	3.00	W.S. Anderson, F. Azhar, P. Kudela, G.K. Bergey, P.J. Franaszczuk. Epileptic seizures from abnormal networks: Why some seizures defy predictability., Epilepsy Research (06 2011)
06/17/2013	4.00	WS Anderson, F Azhar. Predicting Single-Neuron Activity in Locally Connected Networks, Neural Computation (05 2011)
09/02/2014	6.00	Pawel Kudela, William S. Anderson. Computational modeling of subdural cortical stimulation: A quantitative spatiotemporal analysis ofaction potential initiation in a high density multicompartment model., Journal of Neural Engineering (08 2014)
TOTAL:		**5**

Number of Manuscripts:

Books

Received	Book
TOTAL:	

Received	Book Chapter

TOTAL:

Patents Submitted

Patents Awarded

Awards

Graduate Students

NAME	PERCENT_SUPPORTED
FTE Equivalent:	
Total Number:	

Names of Post Doctorates

NAME	PERCENT_SUPPORTED
FTE Equivalent:	
Total Number:	

Names of Faculty Supported

NAME	PERCENT_SUPPORTED	National Academy Member
Pawel Kudela	0.50	
William S. Anderson	0.01	
FTE Equivalent:	**0.51**	
Total Number:	**2**	

Names of Under Graduate students supported

NAME	PERCENT_SUPPORTED
FTE Equivalent:	
Total Number:	

Student Metrics

This section only applies to graduating undergraduates supported by this agreement in this reporting period

The number of undergraduates funded by this agreement who graduated during this period:	0.00
The number of undergraduates funded by this agreement who graduated during this period with a degree in science, mathematics, engineering, or technology fields:.....	0.00
The number of undergraduates funded by your agreement who graduated during this period and will continue to pursue a graduate or Ph.D. degree in science, mathematics, engineering, or technology fields:.....	0.00
Number of graduating undergraduates who achieved a 3.5 GPA to 4.0 (4.0 max scale):.....	0.00
Number of graduating undergraduates funded by a DoD funded Center of Excellence grant for Education, Research and Engineering:.....	0.00
The number of undergraduates funded by your agreement who graduated during this period and intend to work for the Department of Defense	0.00
The number of undergraduates funded by your agreement who graduated during this period and will receive scholarships or fellowships for further studies in science, mathematics, engineering or technology fields:	0.00

Names of Personnel receiving masters degrees

NAME

Total Number:

Names of personnel receiving PHDs

NAME

Total Number:

Names of other research staff

NAME PERCENT_SUPPORTED

FTE Equivalent:

Total Number:

Sub Contractors (DD882)

Inventions (DD882)

Scientific Progress

(1) Forward

This is the final report on ARO grant W911NF-12-1-0418 titled "Biophysical model of cortical network activity and the influence of electrical stimulation". We present a record of our activities during this three-year project dated 15 August 2012 - 14 August 2015. This project was focused on the developing of new methods and modeling techniques allowing for the simulation of active networks subjected to electrical stimulation. The report describes modeling studies that were carried out as an attempt to model and quantify the effects of subdural electrical stimulation on a high-density network consisting of several populations of multicompartment cell types.

(2) Table of Contents

(3) Statement of Problem Studied

This grant aimed to use a biologically realistic network model to investigate how electrical stimulation affects behaviors of the brain's cortical network exhibiting pathologic or physiologic cortical firing patterns. Modeling efforts were focused on providing information in a quantitative manner on the effects of stimulation on cortical network activity and its temporal evolution in the areas adjacent and remote to the stimulating electrode. The onset of focal seizure was modeled in in the built network model and the results derived from these modeling studies were compared with recordings obtained from subdural microwire arrays (for local filed potentials measurements) in humans at the onset of the focal seizures.

(4) Summary of Work Completed

Aim 1) To develop a calibrated computational model of normal and epileptic cortex using multicompartment neuronal representations and an applied external electric field.

This specific aim has been completed. We developed a realistic computational model of cortical network in which the effect of an external electric field can be simulated and investigated. The developed network model represents an unfolded slab of neocortical tissue (4.8 x 4.8 x3mm), consists of a several different types of multicompartmental cortical neurons (excitatory and inhibitory) and encompasses multi-layer structure of cortical circuitry. The developed model is unique and has several advances comparing to other existing models, which include multi-neuronal types and high cell density (103/mm3). The model allows for better quantification of the effects of stimulation in terms of depth, focality, and spatial extent of the recruited neuronal volume by the stimulating electrode as well as for the creation of maps of direct neural activation. In particular, the developed model allows for studying how the effects of stimulation vary across neuronal populations in various neuron types. It allows for identification of axonal sites where presynaptic action potentials are initiated in each neuronal type and for the statistical analyses of these recruited presynaptic action potentials. Based on these analyses, the effect of changing various stimulation parameters on neuronal recruitment across the single neuronal population and types can be assessed. These include the effect of changing the amplitude of the stimulating current and varying the polarity sequence of the charge-balanced pulse. The high

density of neurons in our model, compared to densities in similar previously studied models, permits the quantification of how the electrode size affects the number of recruited neurons. The results of these studies have been published in the October 2015 issue of the Neuromodulation: Technology at the Neural Interface journal[1] and were presented in 2014 Society for Neuroscience Meeting.

Aim 2) To compare the results obtained in our simulation studies with recordings obtained from a new subdural grid design incorporating standard electrode elements and microwires for local field potential measurements during electrical stimulation for cortical mapping to identify context dependent stimulation effects.

This specific aim has been completed. We recorded local field potentials from microelectrode arrays (micro-iEEG) with a millimeter scale spatial resolution during ictogenesis of focal seizures in humans. In parallel, a focal seizure activity was simulated in the cortical network model. The cortical model yielded analogous simulated local filed potentials data (9 or 16 electrodes) with a similar millimeter scale spatial resolution. A multivariate autoregressive (MVAR) model was fitted to simulated and recorded multichannel micro-iEEG data which were treated as one multivariate stochastic process. The MVAR model coefficients were used to calculate spectral measures of causality in the Granger sense and were later used for reconstruction of the seizure propagation pattern. In order to characterize patterns of seizure propagation between microdomains (areas covered by microelectrodes) we analyzed high frequency components (high gamma) in multichannel data obtained from MVAR model. Analyses in high gamma range allow determined dynamic causal interactions between microdomains and consequently reviled pattern of micro propagation of seizure activity inside and outside of the seizure epileptic zone. In addition we compared high frequency micro propagation with those over the surrounding macroelectrodes in low and high frequency bands. The results of these studies have been published in the August 2015 issue of the Journal of Neural Engineering[2] and in the proceedings of the 36th Annual International Conference of the IEEE Engineering in Medicine and Biology Society, EMBC 2014 [3].

(5) Summary of Most Important Results

See PDF file in the attachment

(6) Bibliography

1) Kudela P., Anderson W.S. 2015. Computational Modeling of Subdural Cortical Stimulation: A Quantitative Spatiotemporal Analysis of Action Potential Initiation in a High-Density Multicompartment Model. Neuromodulation 2015; 18: 552–565 doi: 10.1111/ner.12327

2) Basu I, Kudela P, Korzeniewska A, Franaszczuk PJ, Anderson WS. A study of the dynamics of seizure propagation across micro domains in the vicinity of the seizure onset zone. J Neural Eng. 2015 Aug;12(4):046016 doi: 10.1088/1741-2560/12/4/046016

3) Basu I, Kudela P, Anderson WS. Determination of seizure propagation across microdomains using spectral measures of causality. Conf Proc IEEE Eng Med Biol Soc. 2014;2014:6349-52. doi: 10.1109/EMBC.2014.6945080

(7) DD Form 882
See PDF file in the attachment.

Technology Transfer

Our cortical network model developed in collaborations with the Army Research Laboratory, Human Research Directorate, Aberdeen Proving Ground is currently being used to investigate the relationships between blast-related neuronal injuries and large-scale brain network effects (Dr. Piotr J. Franaszczuk and Dr. Jean M. Vettel investigators). These efforts strive towards identifying new robust biomarkers in ECoG/EEG that can aid in determining severity of the injury, monitoring of the progression as well as in predicting the outcome. Results of this work were presented in October 2015 at the Society for Neuroscience Meeting in Chicago, IL.

New promising applications of this cortical model in the context of studying relevant topics for ARL projects are being currently discussed with ARL investigators. This includes a new collaborative project with the ARL based on the ARO 65459-LS proposal for the development of a computational model of auditory cortex and hearing system (Dr. Dana Boatman and Dr. Anderson PIs). This project in addition to experimental studies heavily relies on our cortical network model that has been specially tailored for the needs of auditory cortical system processing.

Summary of Most Important Results

The novelty of these studies is twofold: we can make a prediction about the membrane polarization at each compartment of each individual neuron and at the same time obtain valuable statistical information on the number of recruited neurons along with the initiation sites of the induced presynaptic action potentials (PAPs). This approach differs from earlier studies in which either a lower numbers of neurons were used or just investigated a few neurons positioned in different locations. In contrast to these previous studies, which provided valuable but more qualitative description, our approach allows obtaining a detailed quantitative statistical data about the effects of subdural electrical stimulation.

Neuronal population recruitment

Fig.1 illustrates an example of input-output curves for the axonal activation of pyramidal and basket neurons in supragranular layer II/III obtained for a 0.3 ms long charge-balanced current pulse sequence (anodal-cathodal vs. cathodal-anodal). In the case of pyramidal neurons, PAPs were initiated in either the axon initial segments (with the exception of a low current amplitude < 3 mA) or in the axon branch terminal compartments. The simultaneous occurrence of PAPs in the axon initial segment (AIS) and the axon terminal compartment or in both terminal compartments was observed in less than 6% of activated axons for stimulating currents larger than 3 mA (anodal-cathodal pulse). In contrast, in basket neurons, the initiation of PAPs in the AISs took place only in a small fraction of these neurons and only in the case of cathodal-anodal stimulation (Fig. 1D). In the case of anodal-cathodal pulse stimulation, PAPs in basket neurons were solely initiated in the axon terminal compartments. In the case of cathodal-anodal pulse stimulation, a strong reduction in the numbers of neurons activated in axonal terminals was observed in both pyramidal and basket neurons (Fig. 1C and D)

Lateral and vertical extent of recruited volume

The depth of the spatial extent of neuron recruitment in the vertical direction (perpendicular to the electrode surface) varied for neuron types. Fig. 2 illustrates depth recruitment curves (superimposed) for all types of simulated neurons in supra, inter, and infragranular layers as a function of the applied current amplitude to the electrode for a 0.3 ms long anodal-cathodal (A) and cathodal-anodal (B) pulse sequences. Neuron type specific differences in the depth of recruitment are clearly visible in the infragranular layer where pyramidal neurons in layers V and VI at a given cortical depth

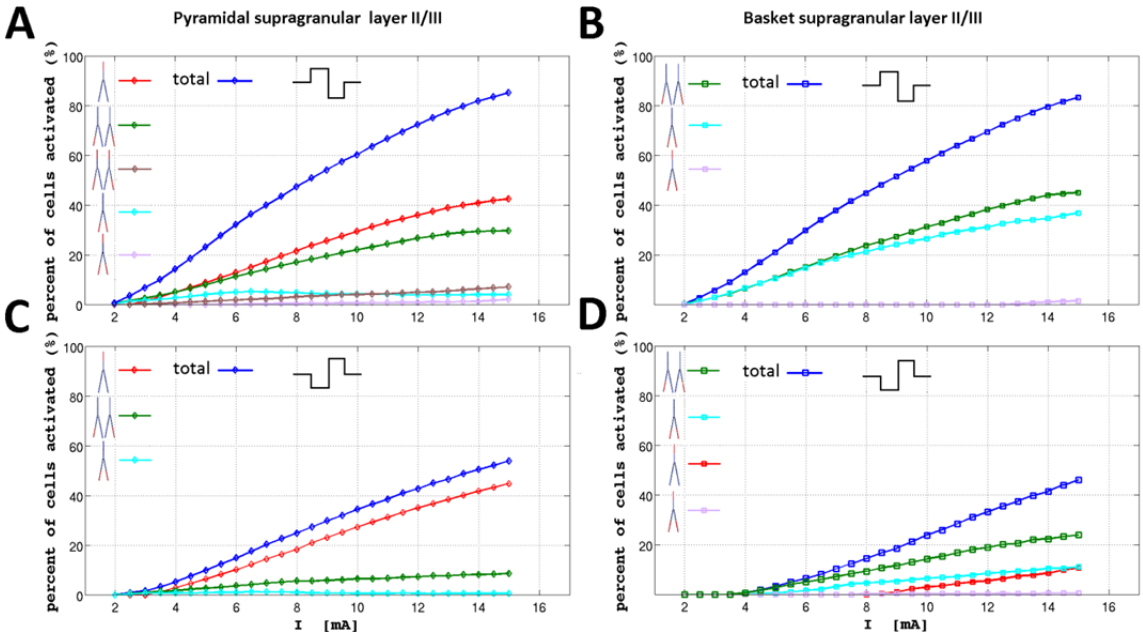

Figure 1 Input-output characteristics of axonal activation for pyramidal (diamonds) and basket neurons (squares) in the supragranular layer (II/III) as a function of the current amplitude (range 2-15 mA) applied to the electrode. Legends (left insets) show neuronal axons along with sites of axonal activations indicated in red. Line color next to the axon matches the corresponding input-output activation curve for a given axonal site. Blue line corresponds to a total number of recruited neurons (sum of input-output activation curves for all axonal sites). A single 0.3 ms long anodal-cathodal (top panels) and cathodal-anodal (bottom) pulse was applied.

need approximately 30% larger current amplitude of the stimulating pulse sequence than basket neurons in order to be activated.

The volume of recruited neurons under the electrode has a radial symmetry and similar to the depth of spatial extend distribution (Fig. 2A and B), the radius of the lateral extent of the recruited neurons can be estimated by measuring the distance between the center of the electrode and the position of the most distal recruited neuron in planes parallel to the electrode surface. Fig. 2C and D show radii of the lateral extent of neuron recruitment under the electrode as a function of the applied current amplitude for all simulated neuron types. With the exception of pyramidal neurons in the infragranular layers, there is a convergence of curves describing the radii of recruitment volumes as the amplitude of the applied current increases (supra- and inter-granular layers).

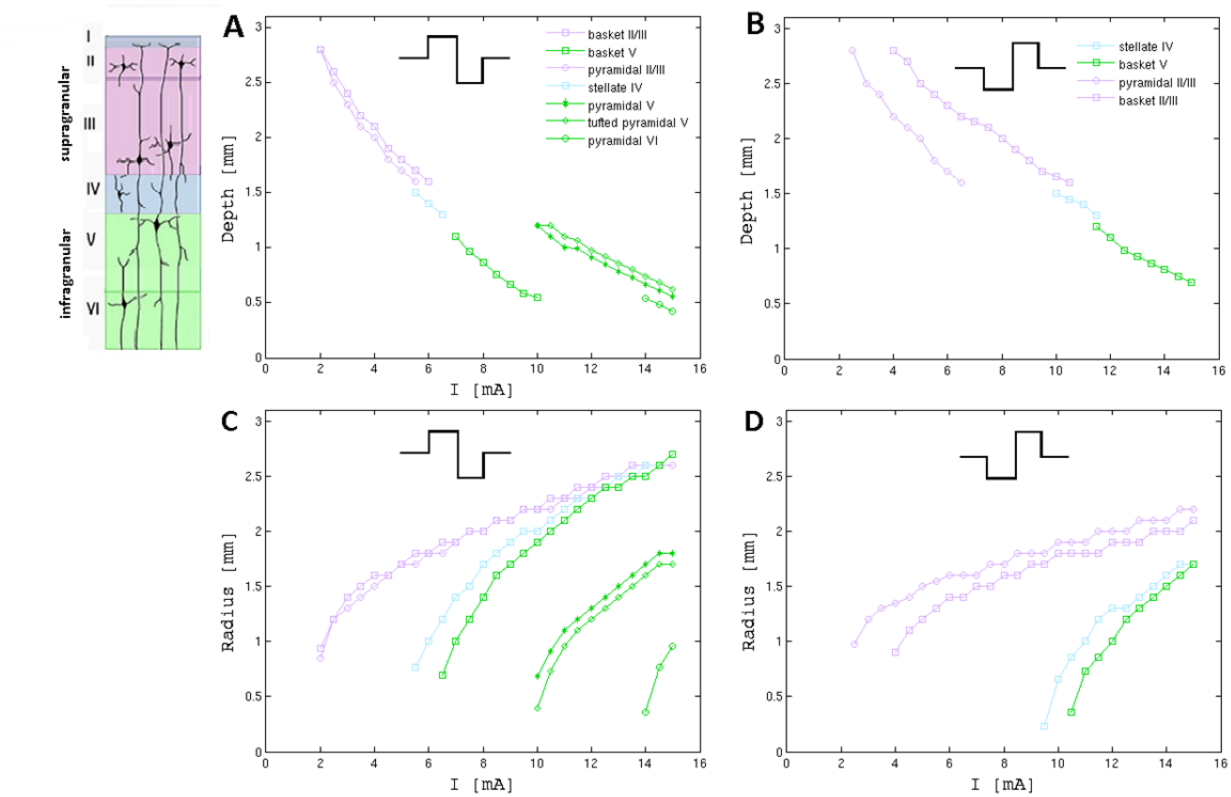

Figure 2 Depths (A,B) and radii (C,D) of a spatial extent of neuron recruitment under the electrode as functions of the applied current. Depths and radii were measured in directions perpendicular and parallel (on a plane) to the pia respectively. Colors of curves correspond to simulated neuron in supra, internal and infragranular layers indicated on left inset.

Pulse polarity sequence

In terms of the total number of recruited neurons the, anodal-cathodal pulse sequence was found to be more efficient than the equivalent cathodal-anodal pulse (Fig. 2A,B and Fig.4A,B,C). The anodal-cathodal pulse as mentioned earlier in general recruited more neurons in the axon terminals than the cathodal-anodal pulse. This can be seen in Figs. 2A and B (green line) as well as in Figs. 4A,B and C (cadet blue colored cloud) where in the case of the anodal-cathodal pulse a considerably larger number of neurons activated in the axonal terminals was observed among all recruited neurons. The anodal-cathodal pulse sequence was also found more effective for the activation of neurons in deeper layers than the analogous cathodal-anodal pulse. This can be seen in Fig. 2A where pyramidal neurons in layers V and VI (green lines) were recruited for $I_0 > 10$ mA by the anodal-cathodal pulse while these neurons were not recruited at all by the equivalent cathodal-anodal pulse (Fig. 2B).

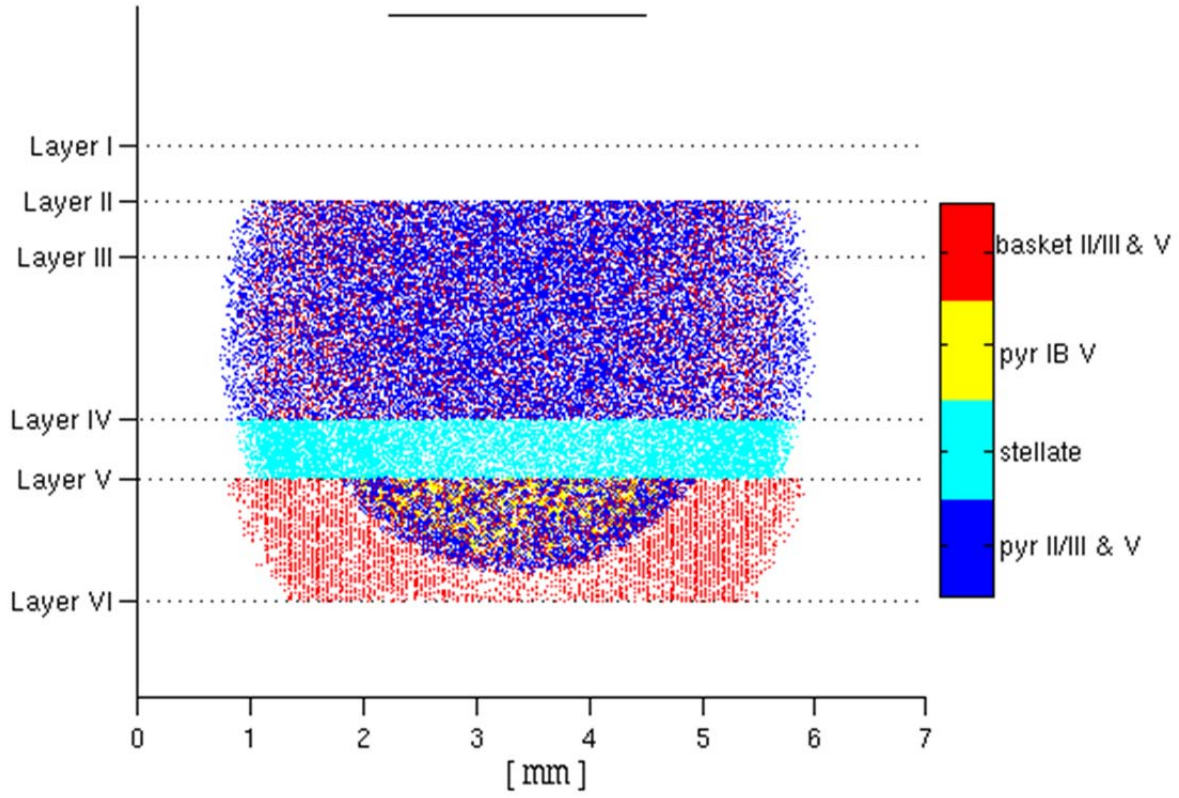

Figure 3 A plot summarizing recruitment of neurons in layers II-V in in a plane perpendicular to the electrode surface and including the electrode center line. The volumes corresponding to recruited neurons (blue - pyramidal, turquoise - stellate, yellow - tufted pyramidal V, red - basket) may overlap (supragranular layer) but in general are not equal. The volumes of recruited pyramidal neurons in the infragranular layer are notably smaller than the volume of recruited basket neurons (red). The position of the electrode is indicated by the top black line. The applied current amplitude was I_0 = 12.5mA and the stimulation pulse was 0.3 ms (anodal-cathodal). The pyramidal neurons in layer VI are not activated at this particular value of I_0 and neurons in layer I were not simulated.

Neuron-type specific recruitment

Curves describing the lateral and vertical extent of the recruited neuron volumes (Fig. 2C and D) depend on neuron type, which suggests that the recruitment volumes will not be identical. The plot summarizing the volumes and distribution of recruited neurons in layers II-V in a plane vertical to the electrode surface including the electrode center line is shown in Fig. 3. In the supragranular layers the volume of the recruited pyramidal neurons (blue) overlaps almost exactly with the volume of recruited

basket neurons (red) which is consistent with Fig. 2C for I_0 = 12.5 mA current amplitude applied to the electrode. The recruitment of neurons in the infragranular layer (V) provides an example of unequal volumes. Particularly the volumes corresponding to the recruitment of two types of pyramidal neurons (regular pyramidal - blue and tufted pyramidal - yellow) lay within the volume of the recruited basket neurons. The latter however extends far beyond the volume of recruited pyramidal neurons.

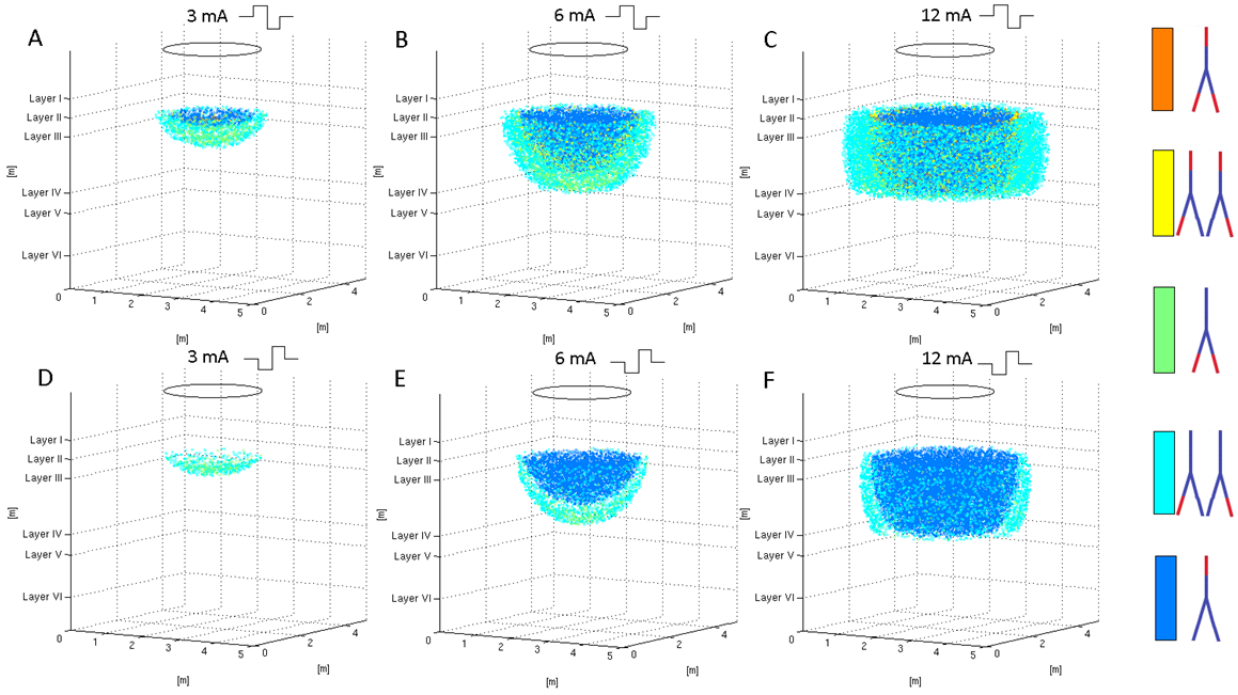

Figure 4 3D maps of recruitment (direct axonal activation) of pyramidal neurons in the supragranular layer by a single 0.3 ms pulse. Stimulating current amplitudes (3, 6 and 12 mA), and stimulus polarization along with the position of the electrode are indicated at the top of each subset. Colors representing the corresponding sites of axonal initiation (indicated in red) are shown on the right.

Sites of PAP initiation

Besides the neuronal class specific differences in neuron recruitment, the response of a neuron to stimulation varies within each neuron type (Fig. 1). The factors affecting the site of initiation of PAPs in a given neuron type include the position and orientation of the neuron relative to the electrode and the amplitude of the applied current to the electrode. Fig. 4 illustrates 3D maps showing the distribution

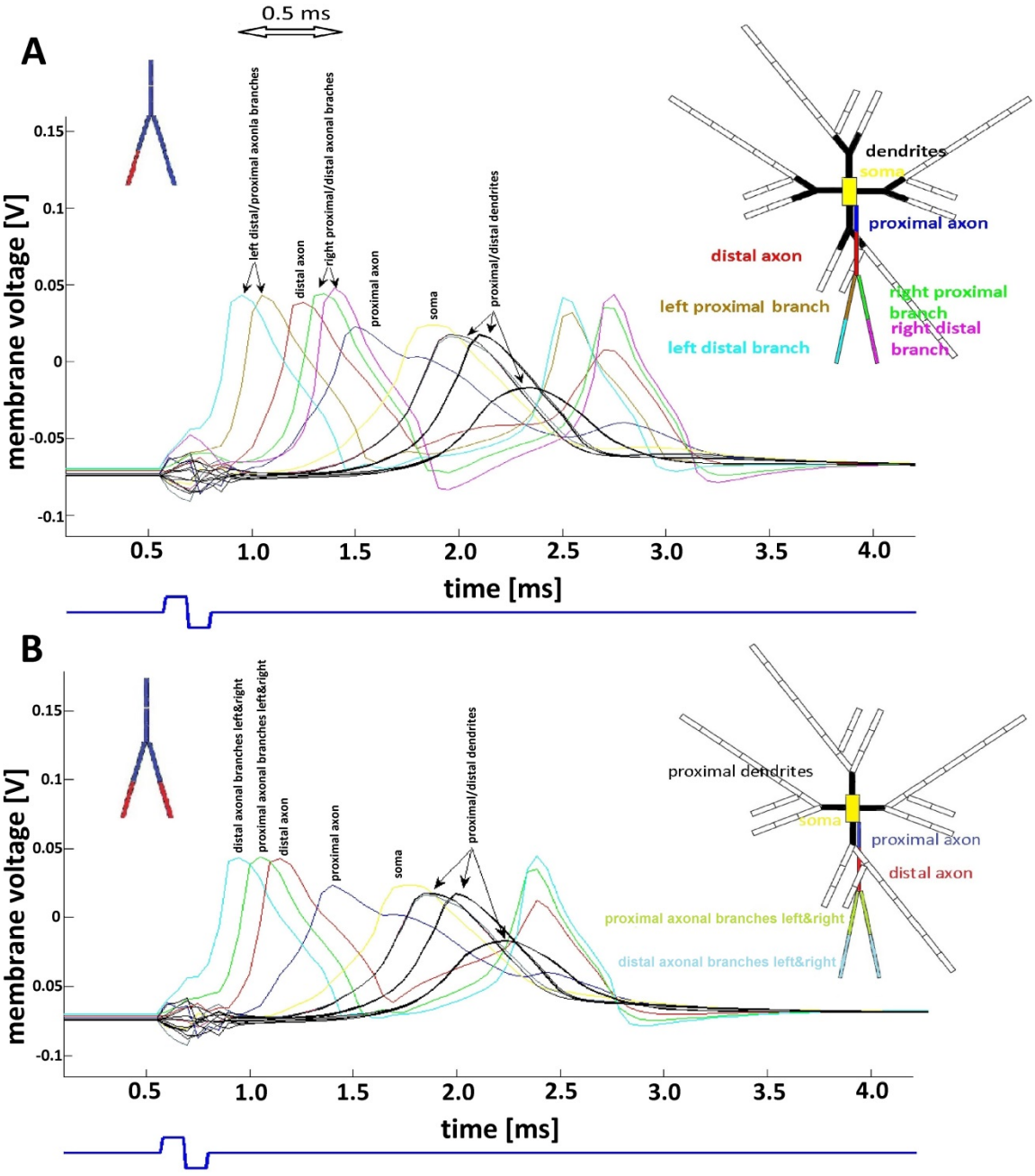

Figure 5 Sequence of excitation of compartments in a model of a basket cell neuron resulting from a single pulse of stimulation. Presynaptic spikes are generated in one (panel A, left top insets shows branch marked in red color) or simultaneously in both distal axonal branches (panel B, left top insets branches marked in red) and propagate antidromically to the soma and later to the dendritic compartments. The second PAP occurs at the axon terminal approximately 1.5 ms after the initial spike and results from orthodromic propagation that follows somatic depolarization (yellow). The pulse timing and duration are indicated at the bottom by the blue trace. In panel A, the PAP is generated in the left distal axonal branch (turquoise) and propagates antidromically towards the distal axon (red) and next to the right axonal branch (green and pink) and somatic/dendritic compartments (yellow/black). Current pulse amplitude in 6 mA; duration 0.3 ms

of sites of axonal AP initiation obtained for pyramidal neurons in supragranular layers and subjected to 3, 6, and 12 mA charge-balanced current pulse sequences (anodal-cathodal and cathodal-anodal). Axons that are closest and directly under the electrode are predominantly activated in AISs (blue core). The initiation within axon terminals takes place solely in the basket like area (light blue/green) that is adjacent and surrounds the core (AIS activation). Simultaneous initiation of PAPs in the AIS and terminal(s) is also demonstrated in Fig. 4 (yellow/orange). These take place mostly in the area between the core and the surrounding basket. It must be noted that the activation maps do not illustrate instantaneous activation of axonal compartments. The points used to create the maps in Fig. 4 were collected over a 4 ms interval after the onset of the stimulation pulse and might be associated with latencies up to 3.1 ms (in the case of a cathodal-anodal pulse). These studies confirmed that the sites of direct activation of neurons are AISs but also indicate that more distal axon segments in the proximity of the AIS (below the first branchpoint) are likely locations where PAPs can originate regardless of the state of the AIS (sup- or sub-threshold activation, hyperpolarization).

Impact of dendritic morphology on axonal activation

After the stimulation, the level of polarization of a given axon compartment depends on the net contribution of current inputs introduced by all the remaining axonal compartments. In the case of the AIS, in addition to the net axonal contribution, the proximal dendritic arbor has a significant impact on the polarization of this compartment. This is different from the activation of the myelinated axon in remote nodes of Ranvier, which are in electrical isolation from the soma or the AIS. The results suggest that despite the relatively high soma->axon resistance (small axon diameter) the mutual somato-dendritic polarization may contribute to the activation of the AIS. Depending on the orientation of a neuron relative to the electrode position and stimulus polarity, different compartments along the neuron will respond with either a positive or a negative polarization of a different magnitude. For the AIS (a perisomatic axonal compartment) it is important whether the net axonal and somato-dendritic current flows make an antagonistic or synergetic contribution. This in turn will be determined by the neuron morphology, orientation relative to the electrode position, and the stimulus polarization. For example the absence of the AIS activation in basket neurons in Fig. 1B by an anodal-cathodal pulse (for comparison see pyramidal neurons in Fig. 1A) can be explained by the morphological differences in the dendritic arborization of basket and pyramidal neurons. The pyramidal neuron model has large diameter apical dendrites and several small diameter basal dendrites. The basket neuron model, contrary to the pyramidal neuron, has four symmetrical (across the neuron main axis) large diameter dendritic branches

(Fig. 5, top right insets). For this stimulation paradigm and the electrode configuration, the neuron's normal axes are perpendicular to the electrode surface meaning that the electric field lines directly under the electrode remain parallel to these axes. The low resistance between the soma, the apical dendritic, and in the case of basket neurons, the basal dendritic branches creates an easy pathway for the flow of axial currents in the direction that is determined by the stimulus polarization. During the anodal stimulation the somal compartment of pyramidal neurons would be more depolarized because a smaller volume of axial current flows into the basal compartments. In the basket neuron, the somal compartment is hyperpolarized rather than depolarized during the same anodal pulse because the current can easily flow into the large diameter and basally oriented compartment. The hyperpolarization of the soma in basket neurons affects the polarization of the AIS by increasing the threshold for activation of this compartment. This may explain the lack of PAP in the AISs in basket neurons subjected to an anodal-cathodal pulse in Fig 1B.

Sealed-end effect in distal axonal compartments

In the case of the most distal axon compartments (below the first branchpoint), in addition to the net current contribution from the adjacent axon compartments, the sealed-end effect will also contribute to the polarization of these compartments. In this stimulation paradigm, the neuron's normal axes are perpendicular to the electrode surface. The axonal terminals will always represent more distal compartments for the neurons (relative to the electrode position) and therefore they will be the most depolarized in the case of anodal stimulation and the most hyperpolarized compartments after cathodal stimulation respectively. This effect is clearly evident in Fig. 1C and D where the number of neurons activated in axon terminals in both types of neurons by cathodal-anodal pulses is lower compared to anodal-cathodal pulses (Fig. 1A,B). There is no rebound excitation in these compartments after the cathodal phase of the stimulus because the width of the pulse phase (0.15 ms) is too short to induce anodal break excitation. This is also evident in Fig. 4D-F where the volume representing activation of axonal terminals is notably smaller.

Temporal response of neurons to stimulation

Analyses of the temporal response of a single neuron to the applied stimulation pulse are illustrated in Fig. 5A and B. The temporal sequences of excitation occurring in neurons are shown by plotting voltage traces in all axonal, somatic, and most proximal dendritic compartments in two basket neurons (A and B) after a 0.3 ms long current pulse. PAPs are initiated in one (A) or simultaneously in

both axonal branch terminals (B). A single stimulation pulse sequence typically induces a PAP duplet at axon terminals, with the second PAP arising from AIS activation by antidromic propagation (towards the soma) from the initial PAP. In panel B, these duplets (the initial and the second PAP) arrive at both terminals at the same time, while in panel A there is latency (0.5 ms) in the arrival of these spike duplets at axonal branch terminals. These results suggests that after stimulation, the time of activation of postsynaptic neurons at presynaptic terminals is not determined solely by the axonal delay (orthodromic propagation) but depends on details of the applied stimulation field. The fact that after stimulation, PAPs arrive at the presynaptic terminals of various branches at different times might be important in characterizing the effects and evaluating the efficacy of electrical stimulation. The temporal variability of PAPs can contribute to desynchronizaton of the neural activity and therefore may underlay desynchronizing or anti-epileptic effects of stimulation.

Electrode diameter

In the current-controlled configuration (constant current) for the simulations used in this work, the electrode diameter has a minor effect on the recruitment of neurons. Fig. 6 illustrates input-output curves of neuronal activation obtained for three different electrode diameters. The slope of the input-output curves as well as the number of recruited neurons are relatively unaffected by the electrode diameter for the 4 -6 mA range of the stimulation current. However the input-output curves diverged for stimulation currents below 4 mA and when the applied current to the electrode is above 6 mA. These results suggest that when the electrode diameter is changed, the total number of recruited neurons does not change notably as long as the current I_0 applied to the electrode remains the same (which is the case in current-controlled stimulation). The modest impact of the electrode diameter on the number of recruited neuron can be explained by the fact that the lateral and vertical extent of the recruited neuron volume is inversely correlated to the electrode diameter. In general, electrodes with larger diameters, besides providing a larger lateral extent of field effects, will offer a smaller extent of the recruitment volume in the vertical direction. Electrodes with smaller diameters will offer a larger vertical field effect but with a smaller lateral extent. The latter suggests that for a given I_0 smaller electrodes will generally provide better recruitment of neurons in the vertical direction. It should be noted that this is only a theoretical supposition because for a given amplitude of I_0 (constant-current stimulation), when the electrode diameter d decreases, the V_0 potential at the electrode will increase as 1/r (r=d/2 is an electrode radius). Therefore small diameter electrodes will require larger V_0 potentials in order to

activate the same number of neurons. For that reason the simulations described in this work with small diameter electrodes *in situ* may be associated with a higher risk of tissue damage since a larger current density will be delivered from a small electrode area.

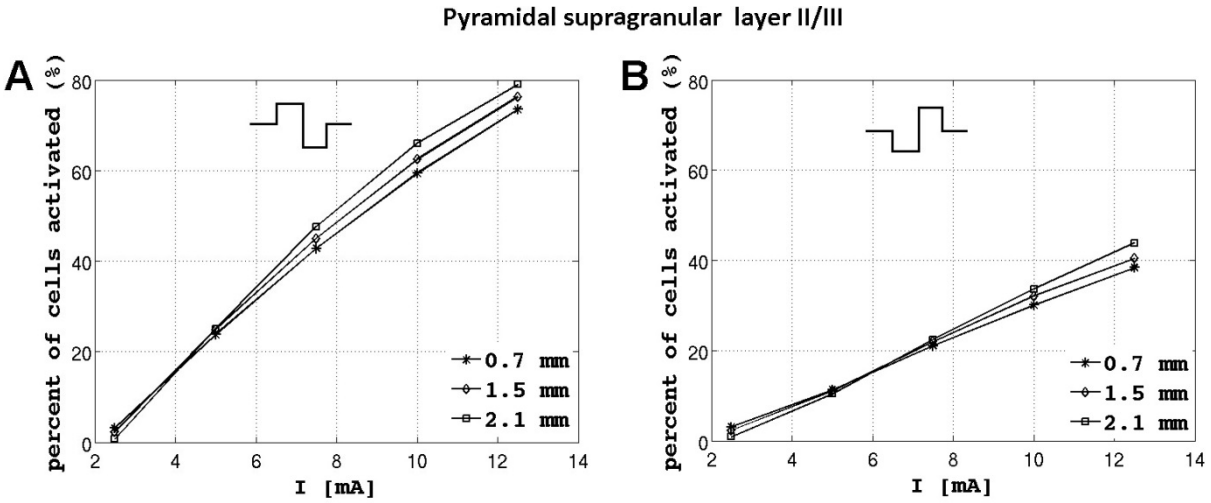

Figure 6 Effect of changing electrode diameter on numbers of activated neurons. Input-output curves of axonal activation for pyramidal neurons in the supragranular layer (II/III) vs. the current amplitude applied to the electrode (range 2.5-12.5 mA) are shown for 0.7, 1.5, and 2.1 mm electrode diameters. A single 0.3 ms long anodal-cathodal (A) and cathodal-anodal (B) pulse was applied.

Simulation of micro-iEEG recording

The cortical model used to simulate micro-iEEG corresponds to a square area of 0.8 × 0.8 mm sampled by five or sixteen microelectrodes with the distance between the microelectrodes 0.4 mm. A simulated region of cortex was represented by layer 2/3 pyramidal cells, spaced at 25 μm in each horizontal direction. The LFP for the model is derived from a weighted average of the current sources summed over the cellular compartments. This includes synaptic currents (AMPA. NMDA), channel currents, and compartment currents. The simulated dataset of micro-iEEG measured from five virtual micro-electrodes was fitted with a multivariate autoregressive model (MVAR). The direct transfer functions (DTF), direct DTF (dDTF), partial direct coherence (PDC) and generalized PDC (gPDC) were calculated and the propagation pattern was determined over 2–30 Hz range as shown in Fig 7. The actual propagation of the wave across the sampled region from the upper right corner to the lower left

corner is shown on the right side of the Fig 7. It can be seen that although all four measures produce similar flow patterns (initiating at right upper corner), DTF has the most accurate and robust estimation.

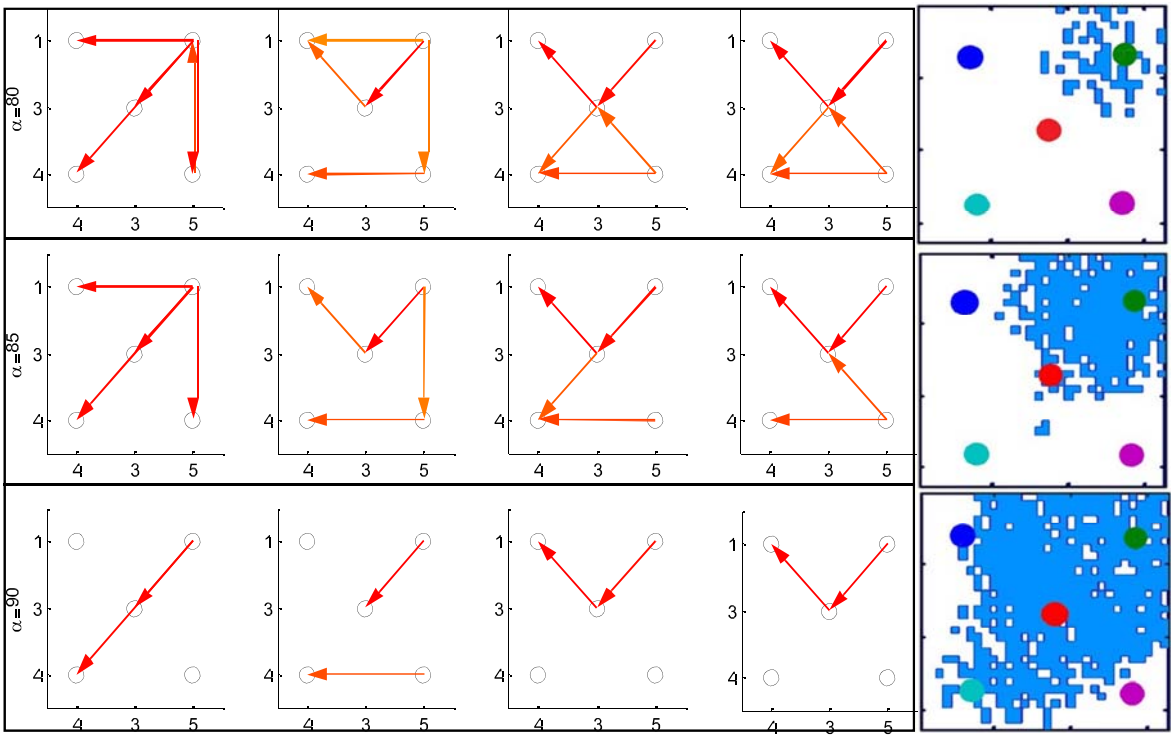

Figure 7. Determination of known propagation (right top to bottom) in simulated five channel micro-iEEG data using DTF, dDTF, PDC and gPDC in the 2–30 Hz frequency band using three values of threshold Tα α = 80,85,90.

Micro-iEEG recording and analyses

The micro-iEEG recorded from 4x4 micro-electrode arrays which were placed within a centimeter of the clinical seizure foci in 4 patients with intractable epilepsy were used to determine the seizure propagation pattern. Each patient had at least 2 micro-electrode arrays, M1 and M2, M1 denoting the one closer to the clinically determined seizure focus than the other (M2) for most patients. We used the DTF measure to calculate propagation over the frequency band determined for each patient by summing over the DTF values in that frequency range.

Positions of the macro-electrode and microelectrode grids are shown in Fig 8. Patients P1 and P2 had left temporal grids (LFT) with two micro-arrays M1 and M2 as shown in Fig 8. Directions of

seizure propagation pattern were determined for each subject (P1-P4). Examples of these analyses are presented below for subject P1 and they can be summarized as follows.

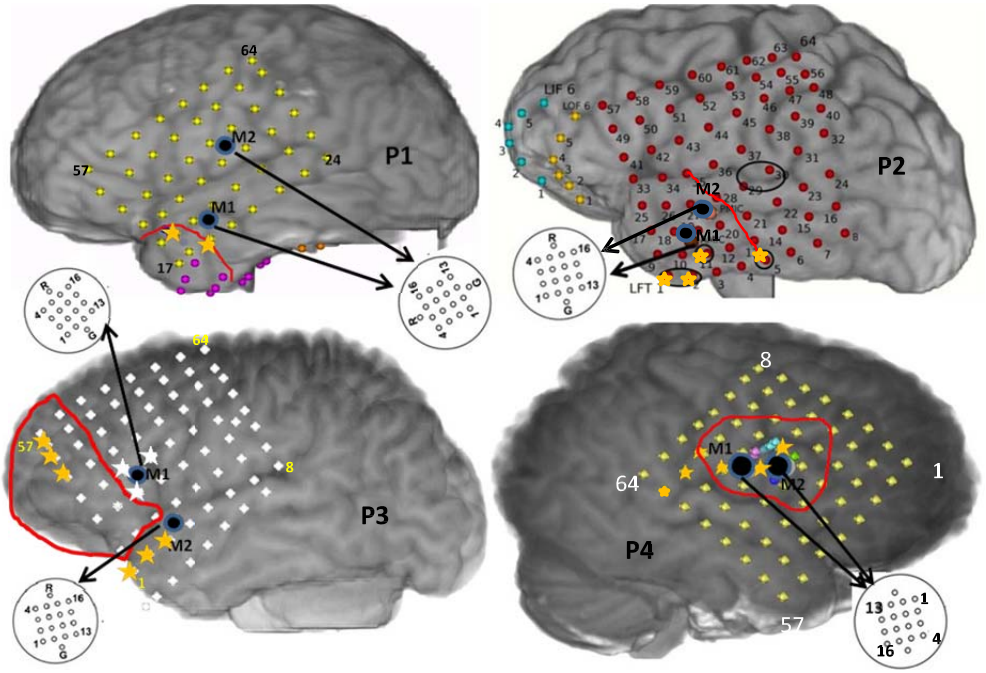

Figure 8. The reconstructed brain maps of the four patients considered showing approximate positions of the macro-electrode and microelectrode grids along with the boundaries of the resected region in red. The yellow asterisks in P1, P2, P4 indicate the seizure onset zone macro-electrode contacts on the grid. The yellow and white asterisks in P3 denote SOZ macro-electrodes during seizures 1 and 2 respectively.

In P1, the earliest seizure onsets on LFT were localized to contacts 19 and 26 as marked by yellow asterisks and the resection boundary with a red line as in Fig. 8. All M1, M2 and LFT 19, 22, 43, 46 channels were used to reconstruct propagation across M1, M2 and the four macro-electrodes surrounding M1, M2 as shown in Fig. 9(A). Fig. 9(D) shows the top four percentile of the thresholded DTF values plotted as propagation across M1 (left corner) and M2 (right corner) along with the strongest flows across the neighboring macro-electrodes in the 4–50 Hz range (green) and 70–110 Hz range (blue). The macro flow over each time window was aggregated and is plotted in Fig. 9(B) with the thickness of the arrows being proportional to the number of flows across a pair of contacts. Both the frequency bands have similar dominant flows except for the top contact pair. Furthermore, the

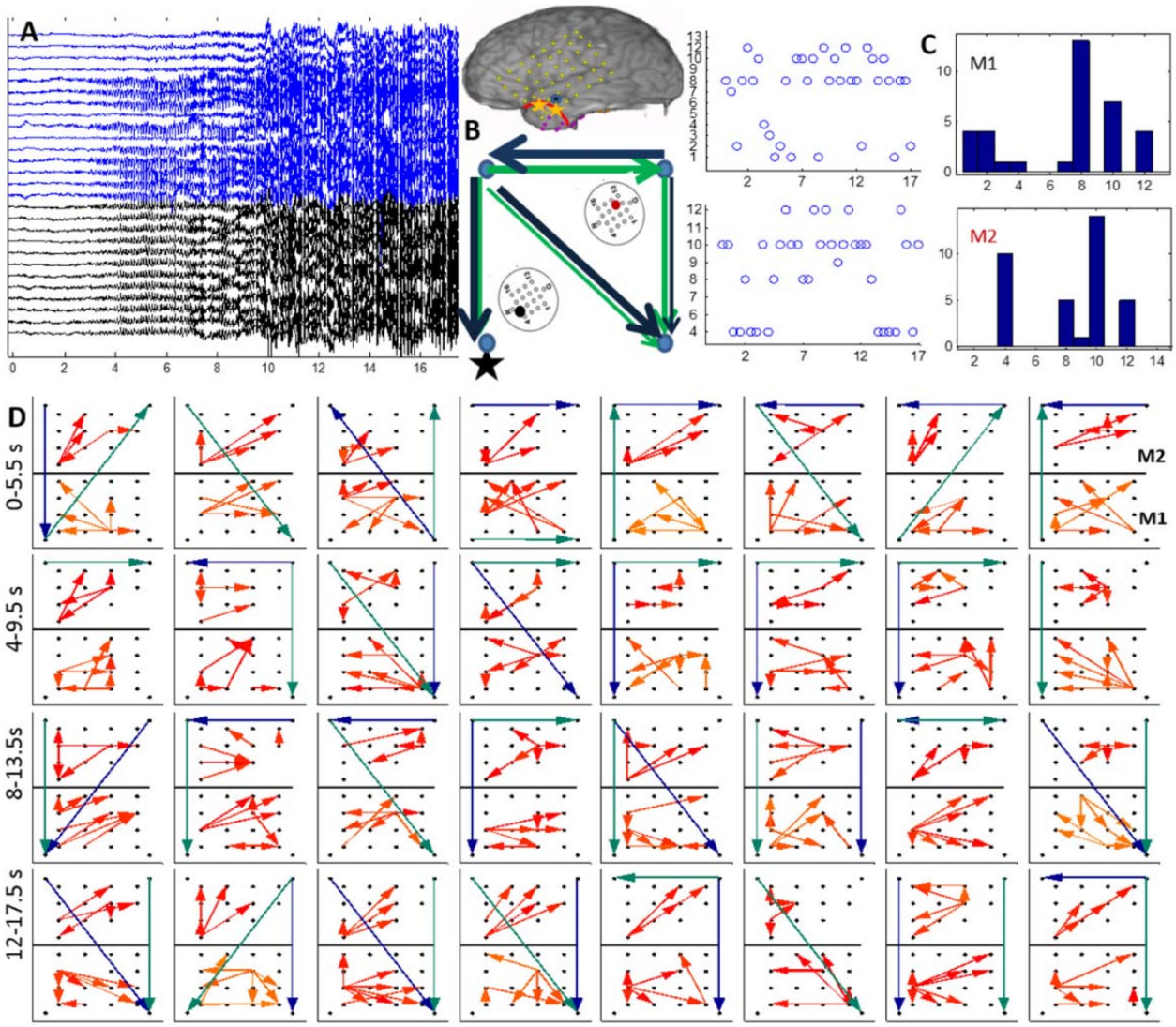

Figure 9. (A) 15 channels of M1 (blue) and 12 channels of M2 (black) recorded from P1 during a clinical seizure, the inset shows a schematic of the implanted grid along with M1 and M2 with the black asterisk denoting the location of the SOZ macro-electrode contact with respect to M1; (B) the 4–50 Hz (green) and the 70–110 Hz (blue) flows in the macro-channels surrounding M1 and M2. The thickness of the arrows is proportional to the number of times a particular direction of flow occurred in the entire interval considered as in (D); (C) time evolution and histogram of micro-electrode contact emanating the maximum outflow within grids M1 and M2 respectively. The channel having maximum outflow for the highest number of times over the entire seizure duration is marked in black and red for M1 and M2 respectively in the schematic in (A); (D) top four percentile of propagation in the 70–90 Hz frequency band across M1 (bottom) and M2 (top) along with the strongest flow across the neighboring macro-electrode contacts in the 4–50 Hz (green) and the 70–110 Hz (blue) frequency bands. Each square element corresponds to a time interval of 2 s and consecutive squares are separated by 0.5 s. The temporal evolution is from left to right. The 32 patterns shown thus correspond to a total duration of 16 s as shown in (A).

channel with the maximum outflow was calculated for M1 and M2 and is plotted over time (left) and as a histogram (right) in Fig. 9(C) which shows that in M1, channel 8 acts as the source for maximum number of time windows whereas in M2, channels 10 and 4 have the highest outflows. From Fig. 4(D), there seems to be a more stable one directional flow pattern in M2 although a single electrode (channel 8) dominates outflow in M1.

Implications for realistic computational models

We used a realistic computational model to generate microelectrode data with a known propagation pattern and the Granger causality measures (DTF, dDTF, PDC, gPDC) to reconstruct the propagation pattern from the simulated data. One of the major challenges of building a realistic computational model for LFPs is calibration and comparison with a measured signal. Although we used a computational model here to validate our propagation reconstruction method, this could also provide a modeling framework for tuning such computational models to match real data in terms of propagation. Efforts focused on reconstruction of pattern of activity propagation between micro-electrodes will potentially play an important role in constructing and validating models of cortical activity, with a reliance on human recordings for calibration. Specifically, these reconstructed patterns from micro-electrodes will help quantify activity spread in lateral direction similar to current density analyses, which allow for studying the laminar pattern of neural activity in neocortex. Therefore details of reconstructed propagation pattern can help in estimation of some values of network parameters which are difficult to determine in situ. These might include selection of weights, numbers, and the range of synaptic contacts in the process of network model parameter tuning in order to reproduce the propagation pattern consistent with measurements of the propagation of epileptiform activity in neocortex.

REPORT OF INVENTIONS AND SUBCONTRACTS

(Pursuant to "Patent Rights" Contract Clause) (See Instructions on back)

Form Approved
OMB No. 9000-0095
Expires Jan 31, 2008

PLEASE DO NOT RETURN YOUR COMPLETED FORM TO THE ABOVE ORGANIZATION. RETURN COMPLETED FORM TO THE CONTRACTING OFFICER.

1.a. NAME OF CONTRACTOR/SUBCONTRACTOR	c. CONTRACT NUMBER	2.a. NAME OF GOVERNMENT PRIME CONTRACTOR	c. CONTRACT NUMBER	3. TYPE OF REPORT *(X one)*
The Johns Hopkins University	W911NF-12-1-0418			a. INTERIM [ ] b. FINAL [X]
b. ADDRESS *(Include ZIP Code)*	d. AWARD DATE *(YYYYMMDD)*	b. ADDRESS *(Include ZIP Code)*	d. AWARD DATE *(YYYYMMDD)*	4. REPORTING PERIOD *(YYYYMMDD)*
733 N Broadway, Suite 117 Baltimore, MD 21205	20120812			a. FROM 20120812 b. TO 20150814

SECTION I - SUBJECT INVENTIONS

5. "SUBJECT INVENTIONS" REQUIRED TO BE REPORTED BY CONTRACTOR/SUBCONTRACTOR *(If "None," so state)*

NAME(S) OF INVENTOR(S) *(Last, First, Middle Initial)* a.	TITLE OF INVENTION(S) b.	DISCLOSURE NUMBER, PATENT APPLICATION SERIAL NUMBER OR PATENT NUMBER c.	ELECTION TO FILE PATENT APPLICATIONS *(X)* d.				CONFIRMATORY INSTRUMENT OR ASSIGNMENT FORWARDED TO CONTRACTING OFFICER *(X)* e.	
			(1) UNITED STATES		(2) FOREIGN			
			(a) YES	(b) NO	(a) YES	(b) NO	(a) YES	(b) NO
N/A	N/A							

f. EMPLOYER OF INVENTOR(S) NOT EMPLOYED BY CONTRACTOR/SUBCONTRACTOR		g. ELECTED FOREIGN COUNTRIES IN WHICH A PATENT APPLICATION WILL BE FILED	
(1) (a) NAME OF INVENTOR *(Last, First, Middle Initial)*	(2) (a) NAME OF INVENTOR *(Last, First, Middle Initial)*	(1) TITLE OF INVENTION	(2) FOREIGN COUNTRIES OF PATENT APPLICATION
(b) NAME OF EMPLOYER	(b) NAME OF EMPLOYER		
(c) ADDRESS OF EMPLOYER *(Include ZIP Code)*	(c) ADDRESS OF EMPLOYER *(Include ZIP Code)*		

SECTION II - SUBCONTRACTS *(Containing a "Patent Rights" clause)*

6. SUBCONTRACTS AWARDED BY CONTRACTOR/SUBCONTRACTOR *(If "None," so state)*

NAME OF SUBCONTRACTOR(S) a.	ADDRESS *(Include ZIP Code)* b.	SUBCONTRACT NUMBER(S) c.	FAR "PATENT RIGHTS" d.		DESCRIPTION OF WORK TO BE PERFORMED UNDER SUBCONTRACT(S) e.	SUBCONTRACT DATES *(YYYYMMDD)* f.	
			(1) CLAUSE NUMBER	(2) DATE *(YYYYMM)*		(1) AWARD	(2) ESTIMATED COMPLETION

SECTION III - CERTIFICATION

7. CERTIFICATION OF REPORT BY CONTRACTOR/SUBCONTRACTOR *(Not required if: (X as appropriate))* [ ] SMALL BUSINESS or [X] NONPROFIT ORGANIZATION

I certify that the reporting party has procedures for prompt identification and timely disclosure of "Subject Inventions," that such procedures have been followed and that all "Subject Inventions" have been reported.

a. NAME OF AUTHORIZED CONTRACTOR/SUBCONTRACTOR OFFICIAL *(Last, First, Middle Initial)*	b. TITLE	c. SIGNATURE	d. DATE SIGNED
Winther, Maili	Grants Associate	Maili Winther	20151211